JOURNAL OF MATERIALS SCIENCE 37 (2002) 2511–2518

Determination of near coincident site lattice orientations in MgO/Cu composite

Y. G. WANG*, Z. ZHANG
Beijing Laboratory of Electron Microscopy, Institute of Physics and Center for Condensed Matter Physics, Chinese Academy of Sciences, P.O. Box 2724, Beijing 100080, People's Republic of China
E-mail: ygwang@blem.ac.cn

G. H. YAN
Department of Physics, Liaoning University, Shenyang 110036, People's Republic of China

J. TH. M. DE HOSSON
Department of Applied Physics, Materials Science Center, University of Groningen, Nijborgh 4, 9747 AG Groningen, The Netherlands

Orientation relations between MgO precipitates and Cu matrix have been characterized by electron diffraction. Four orientation relations were newly found to be coincident with Σ41 [110], Σ13 [111], Σ29 [100] and Σ35 [112] near coincidence-site orientations. The possible dislocation network for these orientation relations was analyzed using O-lattice theory. The size of MgO precipitates with these orientations are in a range of 0.5–1 micron. Frequently appearance of these special orientation relations implies that they may be the favorable orientations for precipitation and coarsening of MgO particles to some extent.

1. Introduction

The research interest of metal-oxide heterointerface stems from the fact that the interface playing an important role in the application of many advanced technologies such as microelectronic package, structural composites and ceramic coatings on metals for abrasion or corrosion protection and sometime being the controlling features in the macroscopic properties of the materials [1–4]. The actual process of joining a metal and an oxide strongly influences the nature of the interface: the macrostructure, the type of orientation, the chemistry and the fine structure in the bonding plane. Consequently a fundamental study and a basic understanding of the fine structure and the properties of metal-oxide composite interfaces is of importance from both scientific and technological points of view. A Cu-MgO composite having a misfit of lattice constant up to 14.2% can be manufactured along two different routes: internal oxidation of CuMg alloys, giving magnesium monoxide precipitates inside copper grains, and internal reduction of (Mg,Cu)O, producing copper precipitates inside magnesium monoxide grains. In the case of internal oxidation several orientation relations between MgO precipitates and Cu matrix have been detected. Dislocations due to misfit at semicoherent interphase boundaries are geometrically necessary defects, which are part of the interfacial structure. Existence of such dislocations was first predicted by Frank and van der Merwe, van der Merwe and van der Merwe *et al.* who described a number of their important properties [5–9]. These dislocations reduce misfit strain energy and, with respect to the unrelaxed interface, they increase interfacial coherency by producing local relaxations. A valuable review on the dislocations in various types of systems, including thin films or islands on substrate, and internal precipitates, was given by Ernst [1].

The objective of the present work is to detect the orientation relations of MgO precipitates with respect to Cu matrix and investigate possible dislocation network in Cu/MgO using O-lattice for these orientation relations.

2. Experimental procedure

Cu-2.5 at.% alloys were cold rolled into ~200 micron thick sheet and internally oxidized at 950°C for 5 hours in a mixture of Cu_2O, Cu and Al_2O_3 powders sealed in an evacuated quartz tube [10]. TEM sample were prepared by cutting 3 mm discs, followed by grinding, dimpling and ion milling to perforation. A JEOL-2010 transmission electron microscope was used at 200 kV for the examination of the microstructure of MgO/Cu composite.

3. Results and discussion

3.1. Examination of crystallographic orientation relationships

Fig. 1 is a composite electron diffraction pattern with incident electron beam parallel to the common [110] zone

*Author to whom all correspondence should be addressed.

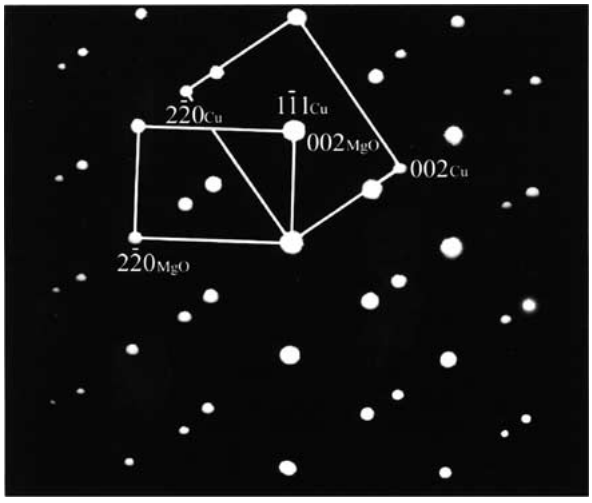

Figure 1 A composite electron diffraction pattern with electron beam parallel to the common [110] zone axis showing MgO precipitates misoriented through ∼55° around [110] axis with respect to Cu matrix, which coincides with Σ41 CSL orientation.

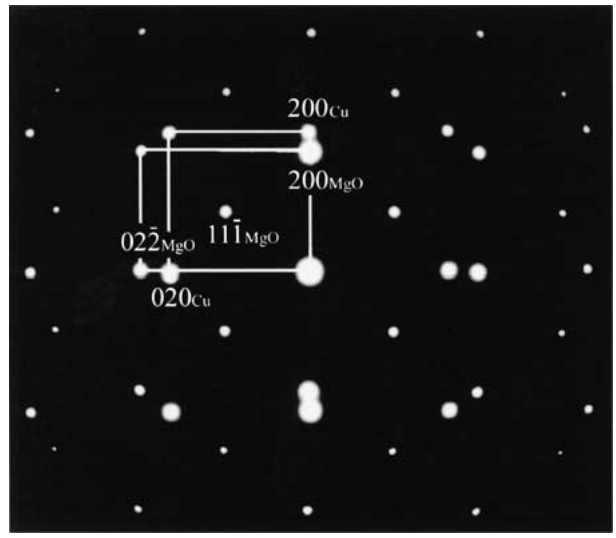

Figure 3 An electron diffraction pattern obtained with electron beam projected along the $[011]_{MgO}//[001]_{Cu}$ direction depicting MgO rotating through ∼44° around the common [100] axis, which results in the Σ29 CSL orientation between MgO precipitate and Cu matrix.

axis, showing a new orientation relation. This pattern can be obtained by rotating the MgO precipitate initially assigned in the cube-on-cube arrangement around the [110] lattice direction through about 55°. Such an orientation relation has been reported in MnO/Cu system [11]. This rotating angle equals to the misorientation angle of 55.88° for Σ41 [110] [12]. Fig. 2 taken with the electron beam incident along the $[\bar{1}\,10]_{Cu}$ and $[\bar{1}\,2\,\bar{1}]_{MgO}$ directions shows another orientation relation, in which there exists a relative rotation of about 30° around the common [111] axis. This orientation relation coincides to Σ13 [111], which needs a deviation of 27.79° from the cube on cube orientation [12]. The diffraction pattern shown in Fig. 3 taken with the electron beam projected along the $[001]_{Cu}$ and $[011]_{MgO}$ zone axes depicts another orientation relation. The feature of this figure is that the [100] axis is common for the two phases and $[01\,\bar{1}]_{MgO}$ parallel to the $[010]_{Cu}$, which is nearly coincident with Σ29 [100] that needs a misorientation of 43.60° from topotaxial orientation [12]. Fig. 4 shows a misorientation about 34° around the common [211] zone axis, which coincides with Σ35 [211] orientation that needs a rotation of 34.05° around this common axis [12]. Coincidence-site lattices are of importance in connection with the study of grain boundaries. Although interface boundaries are two-dimensional features, it is useful to investigating three-dimensional configurations of the interpenetrating point lattices of the host matrix and precipitate and later interpret the interface boundary as a two-dimensional section through this configuration. In general, it is expected that a high-angle interface is favored energetically if the coincidence sites are dense in the plane of the interface. One reason for us to look at the arrangement of coincidence points in three-dimensionalspace and not just in a given plane is that the spatial arrangement for a given rotation allows us to recognize at once all the planes with a high

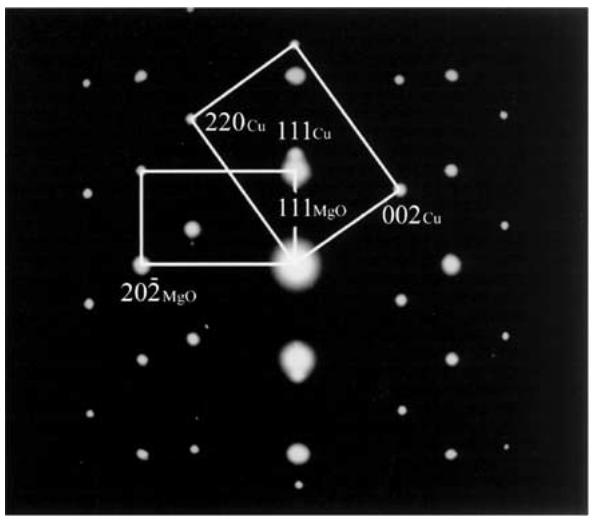

Figure 2 An electron diffraction pattern taken with incident beam along the $[\bar{1}\,10]_{Cu}$ and $[\bar{1}\,2\,\bar{1}]_{MgO}$ directions exhibiting a misorientation of ∼30° [111] MgO relatively to Cu, which forms the near Σ13 CSL arrangement.

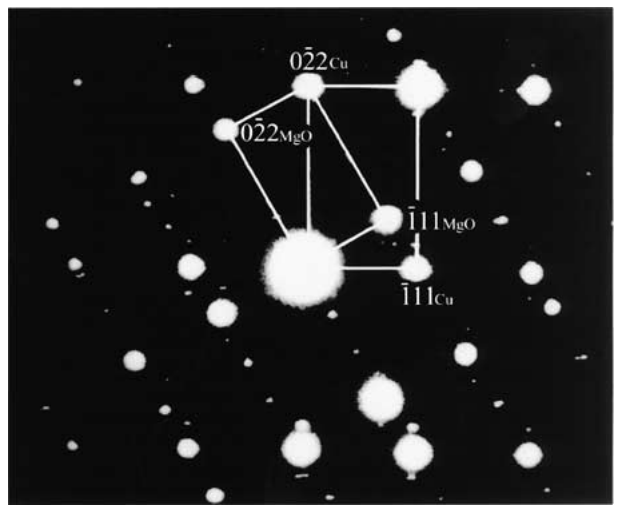

Figure 4 The diffraction pattern with incident beam parallel to the common [211] zone axis demonstrating rotation of MgO precipitate through ∼34° around this common axis, Σ35 CSL arrangement is resulted from such a rotation.

density of coincidence sites. This is important because the interface between two phases may not be planar.

Inspection of samples revealed a wealth of orientation relations. They were all discovered by imaging the Cu along the ⟨100⟩, ⟨110⟩ and ⟨112⟩ directions. No less than 4 orientations have been found to date [13, 14], and it is likely that still more remain to be discovered. Many of these precipitates have interfaces parallel to ⟨110⟩ and ⟨111⟩, which means that there are a large number of very different interfaces present. Over hundred precipitates have been examined, the detected orientation relations and their appearing frequency are list in Table I. It is interesting to note that of all these orientation relations only two or three have also been encountered in a high frequency.

TABLE I Coincident site orientation relations determined in MgO/Cu system

Sigma value	Rotation axis	Rotation angle (deg.)	Appearing frequency (%)
13[a]	⟨111⟩	27.79	9
29[a]	⟨100⟩	43.60	7
41[a]	⟨110⟩	50.47	10
35[a]	⟨211⟩	34.05	6
1	Any	0	45
3	⟨111⟩	60	20
21	⟨211⟩	44.41	3

[a]Determined in this study.

3.2. Morphology of MgO precipitates

The morphology of the MgO precipitates with these orientations was investigated. Fig. 5a to d present a general view of configuration of these precipitates. A perfect octahedron viewed down the ⟨110⟩ and ⟨211⟩ directions is shown in Fig. 6a and b respectively and coincides with a diamond and rectangle shape individually. Comparison of Figs 5 to 6 the MgO precipitates are obviously deviated from the octahedron configuration due

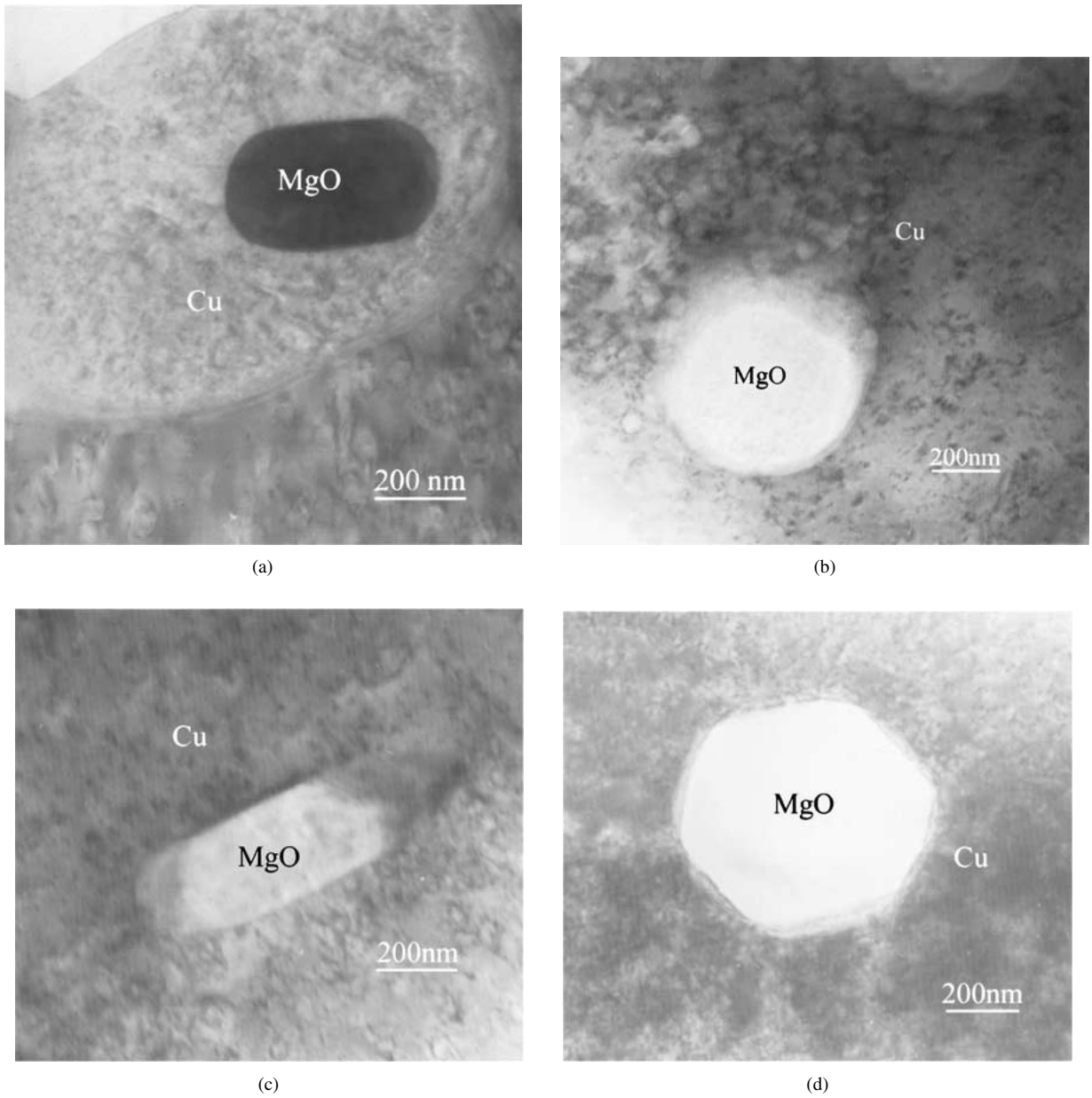

Figure 5 Bright field micrographs taken along different zone axes show the morphology of MgO precipitates with various near CSL orientations respectively, (a) Σ41 CSL, (b) Σ13 CSL, (c) Σ CSL and (d) Σ35 CSL.

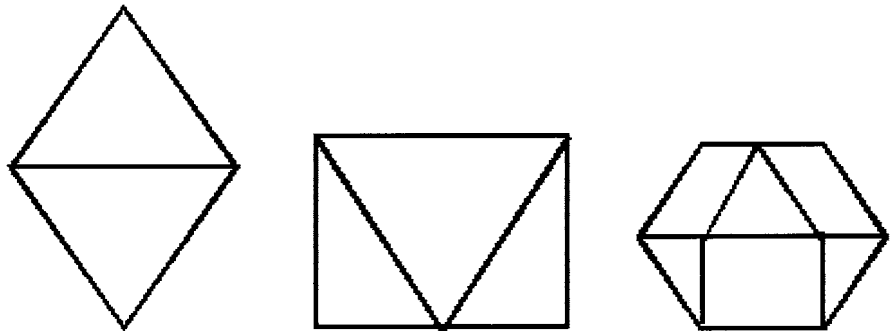

Figure 6 The shapes of a perfect octahedron projected along the (a) ⟨110⟩ and (b) ⟨211⟩ directions, respectively, and (c) is a cuboctahedron with a ratio $\gamma = 0.87$ viewed along the ⟨211⟩ direction.

to the truncations at the corners of the octahedron happened during coarsening of the precipitates. In Fig. 5a and c it can be seen that the {110} planes are well developed during the coarsening of MgO precipitates and the interfaces coincident with theses planes, whereas {111} planes are not sharp with respect to the {110} planes. The {100} planes are found to be the major planes for the truncation on the corners of the octahedron of MgO precipitates. An octahedron truncated by multiple planes can change the shape considerably. Considering the precipitates to be in thermal equilibrium, disregarding strain, and by defining a mean interface energy γ_{100} for the truncated corners and γ_{111} for the {111} facets equilibrium shapes of the precipitates at certain ratios $\gamma_{100}/\gamma_{111}$ can be calculated, by minimizing the total interface energy. Fig. 6c is a cuboctahedron, viewed down the [211] direction, with a ratio of $\gamma_{100}/\gamma_{111}$ equal to 0.87, which looks to be coincident with the Fig. 5d. Configuration of MgO precipitate in Fig. 5b implies that multiple truncation with different ratios of the truncated planes and {111} planes on the corners of octahedron happened during evolution of MgO particle.

Fig. 7 is a [110] high resolution image showing atomic structure of Σ41 CSL orientation. Edge dislocations due to misfit are indicated, where two or three {111} plane spacings in MgO corresponding to three or four {002} plane distances are found. There is not a distinct interface between two phases, but the atomic steps at the interphase interface is obviously revealed. Fig. 8 is a high resolution image taken along the $[\bar{1}10]_{Cu}//[\bar{1}2\bar{1}]_{MgO}$ direction for Σ13 CSL orientation. The interface still coincident with the common {111} plane in two phases is very flat and no step at atomic scale is found at the interface. Viewing along the ⟨211⟩ direction, the {022} planar spacings (0.13 nm and 0.15 nm for Cu and MgO, respectively) are just beyond the resolution of the electron microscope used in this study. Thus, the mismatch dislocations are not clearly revealed.

For high temperature oxidation it is believed that the vacancies necessary to enable the large dilatation connected with the oxide formation are supplied by diffusion or creep processes from surfaces or grain boundaries relatively easily. Volume accommodation is not expected to determine the growth rate. Vacancies are only needed at the oxidation front; behind it coarsening and growth may take place by diffusion in a short range. For fcc structure density of atoms is highest at the {111} planes. If deviated from cube-on-cube and

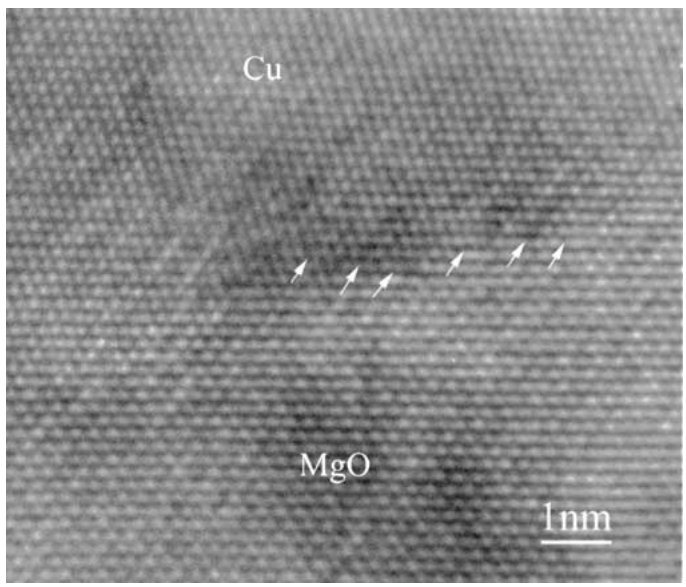

Figure 7 The high resolution image taken along the common [110] zone axis showing mismatch of Cu and MgO at the interphase interface of Σ41 CSL orientation, two $(1\bar{1}1)$ plane spacing in MgO corresponding to three (001) plane distance in Cu are indicated by arrows.

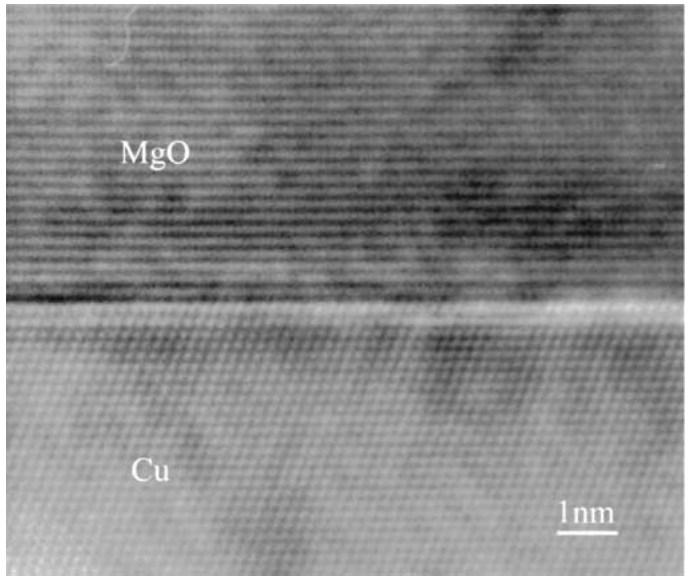

Figure 8 The high resolution image taken along the $[\bar{1}\,2\,\bar{1}]_{MgO}//[\bar{1}\,10]_{Cu}$ direction shows the interface at atomic scale for $\Sigma 13$ orientation.

$\Sigma 3$ orientations or the rotation axis not coincident with the $\langle 111\rangle$ axis, the {111} planes in two phases are not parallel and not the interface, which results in reduction of atomic density at the new interface. As a result there will be more vacancies at the interfaces, which may be favorable for diffusion and coarsening of the precipitates. Elastic strain related with the volume expansion may be relieved. Minimization of interfacial energy is therefore thought to determine the shape of the precipitates. Inside fcc metal MgO often forms a precipitate with truncated octahedral shape. The shape of these precipitates seems to depend on the metal matrix surrounding it. For MgO in Pd and Cu {100} facets have been observed, whereas this is not possible for precipitates in Ag [1, 13, 15]. A precipitate bounded only by {111} planes is a perfect octahedron, and a precipitate surrounded only by {100} planes a perfect cube. At equal volume, an octahedron has a smaller surface than a cube. However, intermediate shapes, consisting partly of {111} planes, {100} planes and {110} can have a smaller surface area than that either octahedron or cube. If the interface energy at the {100} planes is higher than that of the {111} planes, an intermediate shape may still show a smaller interfacial energy than a perfect octahedron.

3.3. O-lattice calculation

In order to visualize the structure of possible misfit dislocation networks at heterointerfaces the O-lattice formulation has been widely used [16–20]. The O-lattice can be calculated as following three steps:

1. A pair of cells, **M1** and **M2**, In the strian-free lattice 1 and 2, respectively, are defined which almost match each other in shape and size.

2. The DSC-1 and DSC-2 lattices for lattice 1 and 2 respectively are then defined. Two new lattices $2'$ and $1'$ are defined.

$$\mathbf{X}_2 = \mathbf{A}\mathbf{X}_1 \qquad \mathbf{X}_2' = \mathbf{A}^{-1}\mathbf{X}_2 \qquad \mathbf{X}_1' = \mathbf{A}^{-1}\mathbf{X}_1 \quad (1)$$

The lattice 1 and lattice $2'$ then form average DSC-1 lattice while lattice 2 and lattice $1'$ form average DSC-2 lattice.

3. The O-lattice produced by DSC-1 and DSC-2 lattices by finding a transformation matrix **T** between these two lattices.

$$\mathbf{X}^{(0)} = (\mathbf{I} - \mathbf{T}^{-1})^{-1}\mathbf{B} \quad (2)$$

where **B** is the matrix of the Burgers vectors of the average DSC lattice.

For the $\Sigma 41$ [110], $\Sigma 13$ [111], $\Sigma 29$ [100] and $\Sigma 35$ [211] relations the rotations matrix **R** can be found in reference [12], they are

$$1/41\begin{pmatrix} 32 & 9 & 24 \\ 9 & 32 & \overline{24} \\ \overline{24} & 24 & 23 \end{pmatrix}, \qquad 1/13\begin{pmatrix} 12 & \bar{3} & 4 \\ 4 & 12 & \bar{3} \\ \bar{3} & 4 & 12 \end{pmatrix},$$

$$1/29\begin{pmatrix} 29 & 0 & 0 \\ 0 & 21 & \overline{20} \\ 0 & 20 & 21 \end{pmatrix}, \qquad \text{and } 1/35\begin{pmatrix} 33 & \bar{6} & 10 \\ 10 & 30 & \overline{15} \\ \bar{6} & 17 & 30 \end{pmatrix}$$

respectively. The O-lattice formed by the DSC-1 and DSC-2 lattices for Cu matrix and MgO precipitate. The DSC-1 and DSC-2 lattices are now the DSC lattices of Cu and MgO respectively. For the $\Sigma 41$ [110] misorientation a basic set of three independent DSC Burgers vectors can be written as

$$\mathbf{B} = (\mathbf{b}_1, \mathbf{b}_2, \mathbf{b}_3) = 1/41\begin{pmatrix} 19 & 4 & \bar{3} \\ 22 & \bar{4} & 3 \\ \bar{4} & \bar{3} & \bar{8} \end{pmatrix} \quad (3)$$

where $\mathbf{b}_1$, $\mathbf{b}_2$ and $\mathbf{b}_3$ are the vectors of primitive unit cell of the DSC lattice for $\Sigma 41$ [110] misorientation [12]. In the same way the three independent DSC Burgers vectors for $\Sigma 13$ [111], $\Sigma 29$ [100] and $\Sigma 35$ [211] orientations can be obtained as following:

$$1/13\begin{pmatrix}5 & \bar{3} & 1\\ 6 & \bar{1} & \bar{4}\\ 2 & 4 & 3\end{pmatrix},\qquad 1/26\begin{pmatrix}29 & 0 & 0\\ 0 & 5 & \bar{2}\\ 0 & 2 & 5\end{pmatrix},$$

$$1/35\begin{pmatrix}13 & \bar{8} & 1\\ 5 & 5 & \bar{5}\\ 4 & 11 & 3\end{pmatrix}.$$

Since the transformation matrix **T** between the DSC-1 and DSC-2 lattices is the expansion-contraction matrix **E**, taking Cu as reference system, the O-lattice points coordinates are now given by

$$\mathbf{X}^{(0)} = (\mathbf{I} - \mathbf{E}^{-1})^{-1}\mathbf{B} = (1/\delta)\mathbf{B} \tag{4}$$

where δ is the lattice mismatch between Cu and MgO defined by

$$\delta = (a_{\mathrm{MgO}} - a_{\mathrm{Cu}})/a_{\mathrm{MgO}} \tag{5}$$

The calculated O-lattices for the $\Sigma 41$ [110] and $\Sigma 35$ [211] orientations have a C-face centered orthorhombic structure [12] with lattice constants of $\mathbf{a}^{(0)} = (1/\delta)|\mathbf{b}_1|$, $\mathbf{b}^{(0)} = (1/\delta)|\mathbf{b}_2|$ and $\mathbf{c}^{(0)} = (1/\delta)|\mathbf{b}_3|$. Bravais classes of the O-lattices for the $\Sigma 13$ [111], $\Sigma 29$ [100] orientations are rhombohedral and tetragonal respectively. Table II lists the O-lattices for all encountered orientation relations in MgO/Cu system. There is a common rule to be deduced based on these data. The obtained O-lattice is hexagonal or rhombohedral if rotation axis parallel to ⟨111⟩ direction, the O-lattice coincides to tetragonal if rotation axis aligned along the ⟨100⟩ direction and orthorhombic or monoclinic structure will be resulted for the O-lattice if the ⟨110⟩ and ⟨112⟩ taken as the rotation axes. This is because the symmetries along the rotation axis will remain in the resulted O-lattice. As a result $\bar{3}$ or 3-fold symmetry along the ⟨111⟩ direction results in the O-lattice with hexagonal or rhombohedral structure and 4-fold symmetry along ⟨100⟩ and 2-fold symmetry along ⟨110⟩ direction will introduce the O-lattices with orthorhombic and monoclinic structure

TABLE II O-lattices for the detected orientations in MgO/Cu system

Sigma value	Bravais class of O-lattice	Parameters of O-lattice (nm)	Orientation of O-lattice
1	Cubic	1.7911	$\mathbf{a}^{(0)}$//⟨110⟩
3	Hexagonal	1.0341	$\mathbf{a}^{(0)}$//[11 $\bar{2}$]
		1.4624	$\mathbf{c}^{(0)}$//[111]
21	C-centered orthorhombic	1.2360	$\mathbf{a}^{(0)}$//[102 $\bar{1}$]
		0.5527	$\mathbf{b}^{(0)}$//[1 $\bar{4}$ 2]
		1.2360	$\mathbf{c}^{(0)}$//[$\bar{4}$ 5 $\bar{8}$]
13[a]	Rhombohedral	0.9935	$\mathbf{a}^{(0)}$//[1 $\bar{4}$ 3]
		1.5709	$\mathbf{c}^{(0)}$//[562]
29[a]	Tetragonal	1.0488	$\mathbf{a}^{(0)}$//[052]
		1.7911	$\mathbf{c}^{(0)}$//[[100]
35[a]	C-centered orthorhombic	1.0488	$\mathbf{a}^{(0)}$//[1354]
		1.0488	$\mathbf{b}^{(0)}$//[$\bar{8}$ 511]
		0.4282	$\mathbf{c}^{(0)}$//[1 $\bar{5}$ 3]
41[a]	C-centered orthrhombic	1.8128	$\mathbf{a}^{(0)}$//[1922 $\bar{4}$]
		0.3956	$\mathbf{b}^{(0)}$//[4 $\bar{4}$ $\bar{3}$]
		0.5594	$\mathbf{c}^{(0)}$//[$\bar{3}$ 3 $\bar{8}$]

[a]The same as that in Table I.

individually. The ⟨112⟩ axis existing within the mirror plane may also cause the O-lattice coincident with orthorhombic type if combined with the 2-fold symmetry perpendicular to it.

In order to understand the correlation between the interfacial structure and the macroscopic properties of metal/oxide it is necessary to have an insight into the dislocation structure of the interface. In general the lattice parameters of a metal and an oxide that meet at an interface do not match, leading to a geometrical misfit. If both metal and oxide are unstrained up to the interface there exist a period at the interface that may be much larger than either of the equilibrium lattice periods of metal or oxide, and that normally is also incommensurable with those. In this case the interface is incoherent. It is clear that atoms near the interface do not all have the same local environment and consequently do not have the same energy. Some atoms will be in a more favorable position than the others. Depending on the strength of the interaction some atoms will move to more comfortable sites and the atomic structure near the interface, predominantly that of the elastically softer material, will relax so as to lower the interface energy. If the lattice parameters at the interface would become equal it is possible that all atoms have the same, favorable, local environment. In this case the interface is coherent. However, the fact that work has to be exerted on system to bring the lattices into registry, leads to an energy balance. In practice an interface is usually neither incoherent nor coherent, but semi-coherent. The interface is in that case characterized by regions in which coherence has increased, and region in which coherence has decreased. Because the misfit is concentrated in the latter regions and because they resemble dislocations, they are called "misfit dislocations". These misfit dislocations at metal-oxide interfaces, unlike the dislocations in the bulk, are not defects but an integral part of the interfacial structure. Their core structure reflects the bonding across the interface. The physical picture is this: on a weakly bounded, near incoherent interface, the cores are delocalized. At a strongly bounded interface the cores are more localized, and a coherent interface region may form if the dislocation climbs away from the interface to a small "stand off" distance. It is clear that the misfit at the interface plays an important role, because the elastic strain energy needed to achieve coherence at an interface with large misfit will in general be higher than for an interface with low misfit. So, the atomic structure is determined by the interplay between misfit and bonding. Determination of misfit dislocations at metal-oxide interfaces co-ordinate with atomic calculations can therefore be expected to lead to a better understanding of these interfaces between dissimilar materials [1, 21]. At present basic understanding of the interplay between structure and properties of grain boundaries in metals and oxides is still very unsatisfactory but somewhat more advanced as far as general features are concerned.

Three dimensional arrangement of dislocation network for these orientations consists of three arrays of

edge dislocations with Burgers vectors coincident with the types of **bi** ($i = 1, 2, 3$) aligned along the edge directions of the O-lattice respectively. The spacings between these dislocation lines equal to $\mathbf{a}^{(0)}$, $\mathbf{b}^{(0)}$ and $\mathbf{c}^{(0)}$ respectively. Summary of the spatial dislocation networks for the detected orientations was given in Table III.

3.4. Interfacial energy contributed by misfit dislocations

An important property of a metal-oxide interface is its free energy per unit area, and the closely related work of adhesion. Thermodynamic and mechanical properties of the interface have been found to depend on these. Experimental determination of the interface energy is an important step towards understanding of metal-oxide interfaces. The link between the atomic structure and the interface energy is then provided by the interplay which exists at the interface between the bonding across it and geometrical misfit that is present. The free energy of metal and oxide interface is of proportion to the square value of Burgers vector of misfit dislocations. From Table III it can be known that Burgers vectors of the misfit dislocations alter as the directions for some orientations, thus, the linear density of the misfit dislocations can be calculated and listed in Table IV. The dislocation structure for (*hkl*) plane obtained by the intersection of the boundary plane with the Wigner-seitz cell walls of the O-lattice is constructed by combination of these listed dislocations. As a result the interfacial energy contributed by solely misfit dislocations at the (*hkl*) boundary could also be estimated qualitatively by multiplication of these products of the linear density and scale square value of the corresponding Burgers vector of misfit dislocations along the different directions. The orientation relations with the high Σ values except Σ13 could have lower interfacial energy contributed only by the misfit dislocations than the cube on cube and Σ3 twin orientations based on this criterion. O-lattice theory developed only for description of the geometrical mismatch of two lattices may possibly predict the interfacial energy contributed solely by misfit. But it can't be used to predict the total interfacial energy of two phases precisely because elastic strain energy, dislocation reactions such as misfit dislocations dissociasted into misfit partial dislocations [22] and certain facets accommodated with step dislocations, which occur to lower the interfacial energy, can not be described by O-lattice theory. Due to no theoretical data on these energies it is difficult to compare the total interfacial energy between the orientations with the high Σ values and cube on cube and Σ3 twin orientations. Experimentally these orientations with the high Σ values presented in a much lower frequency than the cube on cube and Σ3 twin orientations, it implies that these orientations corresponds to a higher energy with respect to the cube on cube and Σ3 twin orientations.

A slight deviation from a coincident site lattice could result in secondary grain boundary dislocations with Burgers vectors only a fraction of those of lattice dislocations first found by Schober and Bulluffi and named due to this reason [23]. Such dislocations are observed to accommodate with the grain boundaries as well as interphase interfaces of composite and are important because they can minimize the boundary energy if superposed on these boundaries [23, 24]. The feature of secondary dislocation is that it can only exist within the boundary and not branch out into a crystal. Secondary dislocation resulting from deviation from the reported orientation also encountered in MgO/Cu composite [25], which is favorable for minimizing the interfacial energy and coarsening of MgO precipitates with the orientations other than coincident site lattice arrangements.

3.5. Angle between the planes with the same Miller index for the determined orientations

If the orientation deviates from the cube on cube arrangement, the interphase boundaries do not coincide

TABLE III Possible dislocation net for the examined orientations in MgO/Cu system

Sigma value	Burgers vectors	Directions of dislocation lines	Spacings of dislocation lines (nm)
1	1/2⟨110⟩	⟨110⟩	1.79
3	1/6⟨112⟩	⟨112⟩	1.03
	1/3⟨111⟩	⟨111⟩	1.46
21	1/21[1021]	[1021]	1.24
	1/21[1 $\bar{4}$ 2]	[1 $\bar{4}$ 2]	0.55
	1/21[$\bar{4}$ $\bar{5}$ $\bar{8}$]	[$\bar{4}$ $\bar{5}$ $\bar{8}$]	1.24
13[a]	1/13[1 $\bar{4}$ 3]	[1 $\bar{4}$ 3]	0.99
	1/13[562]	[562]	1.57
29[a]	1/29[052]	[052]	0.45
	[100]	[100]	2.53
35[a]	1/35[1354]	[1354]	1.05
	1/35[$\bar{8}$ 511]	[$\bar{8}$ 511]	1.05
	1/35[1 $\bar{5}$ 3]	[1 $\bar{5}$ 3]	0.43
41[a]	1/41[1922 $\bar{4}$]	[1922 $\bar{4}$]	1.81
	1/41[4 $\bar{4}$ $\bar{3}$]	[4 $\bar{4}$ $\bar{3}$]	0.39
	1/41[$\bar{4}$ 3 $\bar{8}$]	[$\bar{4}$ 3 $\bar{8}$]	0.56

[a]The same as that in Table I.

TABLE IV The calculated density of misfit dislocations for various orientation relations in MgO/Cu composite

Sigma value	Burgers vectors	Linear density of dislocations (nm^{-1})	Product of the linear density and $\lvert\mathbf{b}_i/a_{Cu}\rvert^2$
1	1/2⟨110⟩	0.56	0.28
3	1/6⟨112⟩	0.97	0.16
	1/3⟨111⟩	0.68	0.23
21	1/21[1021]	0.81	0.20
	1/21[1 $\bar{4}$ 2]	1.82	0.09
	1/21[$\bar{4}$ $\bar{5}$ $\bar{8}$]	0.81	0.20
13[a]	1/13[1 $\bar{4}$ 3]	1.01	0.16
	1/13[562]	0.64	0.25
29[a]	1/29[052]	2.22	0.08
	[100]	0.40	0.40
35[a]	1/35[1354]	0.95	0.16
	1/35[$\bar{8}$ 511]	0.95	0.16
	1/35[1 $\bar{5}$ 3]	2.33	0.07
41[a]	1/41[1922 $\bar{4}$]	0.55	0.28
	1/41[4 $\bar{4}$ 3]	2.56	0.06
	1/41[$\bar{4}$ 3 $\bar{8}$]	1.79	0.09

[a]The same as that in Table I.

TABLE V Angle between the planes with the same index for the determined orientations

Sigma value	(100)	(110)	(111)	(112)
1	0	0	0	0
3	48.2°	33.6°	0	11°
21	27.8°	21.8°	14.5°	0
13[a]	22.6°	15.9°	0	9.2°
29[a]	0	30.5°	35.3°	24.8°
35[a]	19.5°	16.8°	27.7°	0
41[a]	38.7°	0	34.9°	27.1°

[a]The same as that in Table 1.

to the planes with the same index for the two phases except the planes perpendicular to the rotation axis. The angle θ between the planes with the same index of the two phases can be calculated as following:

$$\theta = \cos^{-1} \times \frac{\sum_{i=1}^{3}\sum_{j=1}^{3} a_{ji}h_j h_i}{\sqrt{\sum_{j=1}^{3} h_j^2} \bullet \sqrt{\sum_{j=1}^{3}\sum_{m=1}^{3}\sum_{i=1}^{3} a_{ji}a_{jm}h_i h_m}} \quad (6)$$

where a_{ji} and h_i are the element of rotation matrix relating two sets of basis of MgO and Cu and miller index of the plane respectively. The angle of some planes with low index has been calculated based on Equation 6 and given in Table V.

4. Conclusions

Based on the experimental evidences some orientation relations of Cu matrix and MgO precipitates were newly determined to be coincident with Σ41 [110 Σ13 [111], Σ29 [100] and Σ35 [211] orientations respectively. The morphology of the MgO precipitates oriented in these CSL orientations deviated from the octahedron probably due to the multi-truncations on the {100}, {110} planes etc. Calculation via O-lattice formula shows that the interfacial energy contributed sole by the misfit dislocations for the higher Σ orientations is similar to those of the cube on cube and Σ3 twin orientations, although these higher Σ orientations appeared in a lower frequency than the cube on cube and Σ3 twin orientations.

References

1. F. ERNST, *Mater. Sci. Eng*. R **14** (1995) 97.
2. W. MADER and D. KNAURS, *Acta Met*. **40** (1992) 207.
3. V. VITEK, G. GUTEKUNST, J. MAYER and M. RÜHLE, *Phil. Mag*. A **71** (1995) 1219.
4. W. Z. ZHANG, *ibid*. **78** (1998) 913.
5. F. C. FRANK and J. H. VAN DER MERWE, *Proc. Roy. Soc*. A **198** (1949) 205.
6. *Idem*., *ibid*. **198** (1949) 216.
7. J. H. VAN DER MERWE, *J. Appl. Phys*. **34** (1962) 117.
8. *Idem*., *ibid*. **34** (1962) 123.
9. J. H. VAN DER MERWE, J. WALTERSDORF and W. A. JESSER, *Mater. Sci. Eng*. **81** (1986) 1.
10. F. N. RHINES and A. H. GROBE, *Trans. AIME* **147** (1942) 318.
11. F. ERNST, *Res. Soc. Sym. Proc*. **183** (1990) 49.
12. H. GRIMMER, W. BOLLMANN and D. H. WARRINGTON, *Acta Crystal*. A **30** (1974) 197.
13. P. LU and F. COSANDEY, *Ultramicroscopy* **40** (1992) 271.
14. Y. G. WANG and J. TH. M. DE HOSSON, *J. Mater. Sci. Lett*. **21** (2001).
15. W. MADER and B. MAIER, *J. De Physique* C **1** (1990) 867.
16. P. LU and F. COSANDEY, *Acta Metall. Mater*. **40** (1992) S259.
17. W. BOLLMANN, "Crystal Defects and Crystalline Interfaces" (Springer, Berlin, 1970).
18. R. BONET and F. DURAND, *Phil. Mag*. **32** (1975) 997.
19. G. C. SAVVA, J. S. KIRKALDY and J. WEATHERLY, *Phil. Mag*. A **75** (1997) 315.
20. W. Z. ZHANG, F. YE, C. ZHANG, Y. QI and H. S. FANG, *Acta Mater*. **48** (2000) 2209.
21. F. R. CHEN, S. K. CHIOU, L. CHANG and C. S. HONG, *Ultramicroscopy* **54** (1994) 179.
22. A. TRAMPERT, F. ERNST, C. P. FLYNN, H. F. FISCHMEISTER and M. RÜHLE, *Acta Metall. Mater*. **40** (1992) S227.
23. T. SCHOBER and R. W. BALLUFFI, *Phil. Mag*. **24** (1974) 165.
24. I. MACLAREN and M. AINDOW, *Phil. Mag*. A **76** (1997) 871.
25. Y. G. WANG, G. H. YAN and J. TH. M. DE HOSSON, *J. Mat. Sci. Eng*. A **28** (2001).

Received 23 April 2001
and accepted 14 February 2002